Kobe University Repository : Kernel

PDF issue: 2025-12-05

Template-Assisted Self-Assembly of Colloidal Silicon Nanoparticles for All-Dielectric Nanoantenna

Negoro, Hidemasa
Sugimoto, Hiroshi
Hinamoto, Tatsuki
Fujii, Minoru

(Citation)
Advanced Optical Materials,10(8):2102750

(Issue Date)
2022-04-01

(Resource Type)
journal article

(Version)
Accepted Manuscript

(Rights)
This is the peer reviewed version of the following article: [Negoro, H., Sugimoto, H., Hinamoto, T., Fujii, M., Template-Assisted Self-Assembly of Colloidal Silicon Nanoparticles for All-Dielectric Nanoantenna. Adv. Optical Mater. 2022, 10, 2102750.], which has been published in final form at https://doi.org/10.1002/adom.202102750. Th…

(URL)
https://hdl.handle.net/20.500.14094/0100476497

Template-Assisted Self-Assembly of Colloidal Silicon Nanoparticles for All-Dielectric Nanoantenna

Hidemasa Negoro, Hiroshi Sugimoto, Tatsuki Hinamoto, and Minoru Fujii**

Mr. H. Negoro, Dr. H. Sugimoto, Dr. T. Hinamoto and Prof. M. Fujii
Department of Electrical and Electronic Engineering, Graduate School of Engineering, Kobe University, Rokkodai, Nada, Kobe 657-8501, Japan
E-mail: fujii@eedept.kobe-u.ac.jp

Dr. H Sugimoto
JST-PRESTO, Honcho 4-1-8, Kawaguchi, Saitama 332-0012, Japan
E-mail: sugimoto@eedept.kobe-u.ac.jp

Keywords: Mie resonance, Dielectric nanoparticle array, Silicon nanoparticle, Self-assembly, Nanoantenna, Directional scattering

Abstract

A solution-based bottom-up process to produce one- and two-dimensional arrays of densely-packed spherical nanoparticles (NPs) of crystalline silicon (Si) having the lowest order Mie resonance in the visible range is developed. First, an agglomeration-free solution of Si NPs with a narrow size distribution is prepared. By using grooves fabricated on the surface of a polymer as a template, arrays of Si NPs with different shapes are formed by a template-assisted self-assembly method, and then they are transferred to an arbitrary substrate. To demonstrate proper formation of Si NP arrays, polarization-resolved scattering spectra are measured for different size linear arrays, i.e., a monomer to a pentamer, of Si NPs placed on a silica substrate. The observed spectra are well-reproduced by the numerical simulations. When the polarization direction of incident light is parallel to the array axis, the scattering spectra are strongly modified from that of a Si NP monomer due to near-field coupling of the electric dipole (ED) modes. In a Si NP tetramer, the peak of the ED mode overlaps with that of the magnetic dipole (MD) mode and strong forward scattering is observed at the MD peak wavelength due to the Kerker effect.

1. Introduction

Nanoparticles (NPs) of high refractive index materials such as silicon (Si) supporting the lowest order Mie resonances in the visible to near infrared range attract attention as a platform for manipulating light-matter interaction at the nanoscale.[1] The high-index NPs work as a nanoantenna to enhance fluorescence and phosphorescence of phosphors nearby via the Purcell effect and the electric and magnetic field enhancements. [2–5] High-index NP nanoantennas can control the phase and propagation direction of light, [6,7] and nano-optical Yagi-Uda antennas,[8] waveguides[9] and optical spin sorters[10] have been demonstrated. Furthermore, a variety of highly sophisticated metasurfaces composed of designed arrays of high-index NPs such as metalens with a near-unity numerical aperture [11] and metagratings[12] have been produced. These fast developments of dielectric-NP-based nanoantennas and metasurfaces owes the advancement of micro fabrication technologies represented by of electron-beam lithography.[3,7,11,13,14] The top-down micro fabrication process has many advantages for the production of nanoantennas and metasurfaces such as the high accuracy, the high reproducibility, the high compatibility to semiconductor manufacturing process, etc. However, there remain several limitations. For example, reducing the gap between adjacent NPs to nearly zero, which is required to achieve strong near-field coupling between optical modes of NPs,[3,15–17] is not straightforward. Furthermore, a choice of a substrate is limited and usually a large device is hard to be produced.

In addition to the conventional micro fabrication processes, several new processes have been developed to produce dielectric nanostructures. A dewetting process produces NPs in a large area by melting a film on a substrate, although the shape and the position of NPs are not well-controlled. [18] This problem can be overcome by a templated-dewetting process, in which the position and the size of NPs are determined by a template.[19–21] Similarly, a laser printing process can place NPs in desired positions on a substrate and thus can produce a complicated structure.[17,22,23]

An alternative approach to produce NPs on a substrate is using self-assembly of NPs dispersed in solution.[24] This approach allows us to produce a film of partially-aligned NPs in a large area. By using a template, i.e., template-assisted self-assembly, the position of NPs can be controlled precisely. This method has high scalability and can inherently reduce gaps between NPs to nearly zero.[25,26] For plasmonic NPs such as gold and silver NPs, a variety of structures such as linear arrays[27–29], circular symmetric arrays[27] and periodic arrays[30] have been fabricated for optical waveguides[28] and sensors[29,30] by a self-assembly process assisted by guided templates. NP assemblies produced by a template-assisted self-assembly process can usually be transferred to almost arbitrary substrates,[27,28,30] including flexible substrate and even in liquids[31].

In principle, the template-assisted self-assembly method can be applied to Si NPs if a proper precursor solution is available. The prerequisites for the solution for the self-assembly method are the high colloidal stability, high size uniformity and high shape uniformity of NPs.[32] Unfortunately, many of Si NP samples previously produced[33–35] do not satisfy these requirements, and thus the template-assisted self-assembly method has not been successfully applied for the formation of the assembly. As a result, optical studies of dielectric NP oligomers have been limited to a few kinds of very simple structures such as the dimers accidentally formed by agglomeration of NPs[15,17]. Although interesting phenomena such as strong enhancement of electric and magnetic fields at the gap[36], quenching-free fluorescence enhancement of molecules at the gap[3,37], scattering directionality control in a wide angle range including transverse scattering[13,38], etc., have been demonstrated in NP dimers, development of a process to produce more complicated structures with high yields by controlling the position is indispensable to exploit near-field coupling of dielectric NPs for novel applications.

In this paper, we develop a template-assisted self-assembly method for the production of Si NP arrays. We have recently succeeded in producing colloidal solutions of highly-spherical

crystalline Si NPs 100-250 nm in average diameter with the size distribution as small as ~8% of the average diameter.[39] The solution of size-purified NPs exhibits vivid color due to the Mie scattering [40]. The Si NP solution satisfies all the requirements necessary for the template-assisted self-assembly process. To produce Si NP arrays, we employ linear grooves with rectangular cross sections as guided templates. We show that, depending on the groove width, a linear array, a zig-zag array and a two-dimensional (2D) array of Si NPs are formed by the process. We also develop a process to transfer Si NP arrays to arbitrary substrates such as silica and Au. We study polarization-resolved scattering spectra of different length linear arrays of Si NPs (up to a pentamer) attached to each other. We show systematic changes of the scattering spectra with the length of the array due to the coupling of the electric dipole (ED) modes of NPs. In a Si NP tetramer, the peak of the ED mode shifts to that of the magnetic dipole (MD) mode and strong forward scattering appears at the MD mode peak wavelength due to the Kerker effect.

2. Results and discussion

2.1. Fabrication of Silicon Nanoparticles Arrays

Si NPs were grown in a silicon dioxide (SiO_2) matrix by thermal disproportionation of silicon monoxide (SiO) at 1475°C in a N_2 gas atmosphere. The NPs were then extracted from the matrix by hydrofluoric acid (HF) etching and dispersed in methanol.[39] After exchanging the solvent to water, Si NPs were size-separated by sucrose density gradient centrifugation.[39] Figure 1a shows a water solution of size-separated Si NPs. We can see clear yellowish color due to Mie-scattering of Si NPs. Figure 1b shows a TEM image of Si NPs. The NPs are highly spherical, and the crystallinity is high as can be seen in the lattice fringe in the inset. The average diameter estimated from TEM images is 132 nm with the standard deviation of 16 nm (Figure S1 in the Supporting Information).

In template-assisted self-assembly (Figure 1c), convective flow of the solvent drags colloidal particles toward the edge of the meniscus, and creates a high density accumulation zone.[26,31,41] The high particle density in the accumulation zone suppresses Brownian motion of particles and prevents their escape to the solvent, promoting efficient particle-trap to a template.[41] Figure 1e shows a SEM image of 200 nm-width linear grooves after the template-assisted self-assembly process. Si NPs are aligned in the grooves and the linear array is formed. NPs are attached to each other. The linear arrays are formed when the width of the grooves is slightly larger than the NP diameter. When the width is roughly twice of a NP diameter, a zig-zag array of Si NPs is formed (Figure 1f). In a wider groove, a 2D array of Si NPs, in which NPs are partly regularly aligned, are formed (Figure 1g, h).

Following the template-assisted self-assembly process, Si NP arrays were transferred onto a substrate (Figure 1i). First, ethyl acetate solution of cellulose acetate butyrate (CAB) is deposited on a template and dried in air to form a CAB film. The film is detached from the template in water and placed on a substrate. Dissolution of CAB by ethyl acetate results in transfer of Si NP arrays onto the substrate.

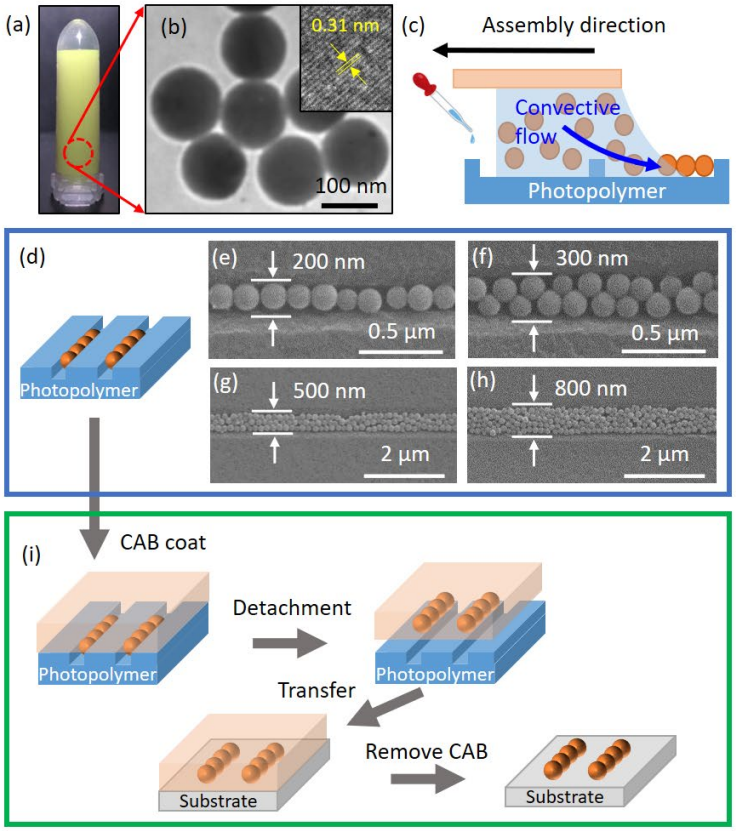

Figure 1. a) A photograph of water solution of colloidal Si NPs (d_{ave} = 132 nm). b) TEM image of Si NPs. Inset is the high-resolution image. c) Schematic illustration of template-assisted self-assembly process. A blue arrow indicates convective flow of solution that drags Si NPs toward the edge of the meniscus, where they are assembled. d) Schematic image of Si NP arrays in grooves of a template. e-h) SEM images of Si NP arrays; e) a linear array in a 200 nm-width groove, f) a zigzag array in a 300 nm-width groove, and g, h) 2D arrays in 500 nm- and 800 nm-width grooves. i) Procedure to transfer Si NP arrays to a substrate.

Figure 2(a-c) shows SEM images of Si NP arrays on a silica substrate produced by using different width grooves. We can see that a linear array (Figure 2a), a zigzag array (Figure 2b) and a 2D array (Figure 2c) of Si NPs are successfully transferred on the substrate and the NPs are attached to each other. Figure 2d and e shows dark field optical microscope images of linear arrays when the polarization direction of incident light is parallel and perpendicular to the axis of the arrays, respectively. The scattering color and intensity depend strongly on the

polarization direction, suggesting near-field coupling of Mie resonance modes of NPs along the array axis due to almost zero gap between NPs.[17] We will discuss the coupling behavior for a monomer to a pentamer of Si NPs in detail.

With this process, we can transfer Si NP arrays onto almost any substrates. To demonstrate this capability, we transfer Si NP arrays onto a flat Au film. A NP placed on a flat metal surface, i.e., a NP on a mirror structure, acts as a nanoantenna with very small mode volume and large field enhancement, and many different shape NPs, i.e., a metal sphere ,[42] a metal cube ,[43] a dielectric sphere ,[44][45] a dielectric wire,[46] etc., are placed on metal surface and the optical responses are studied. However, most of these previous studies focus on single NPs on a mirror, and no systematic studies have been made on dielectric NP arrays on a mirror structure because of the lack of the process to place a NP array on a mirror. Figure 2f shows a SEM image of a Si NP linear array (hexamer) placed on an atomically flat Au substrate by the process shown in Figure 1i. Figure 2g shows a dark field microscope image (random polarization) of a linear array. The scattering color is reddish compared with the case of NP arrays on a silica substrate due to coupling of the resonance mode with the mirror image.

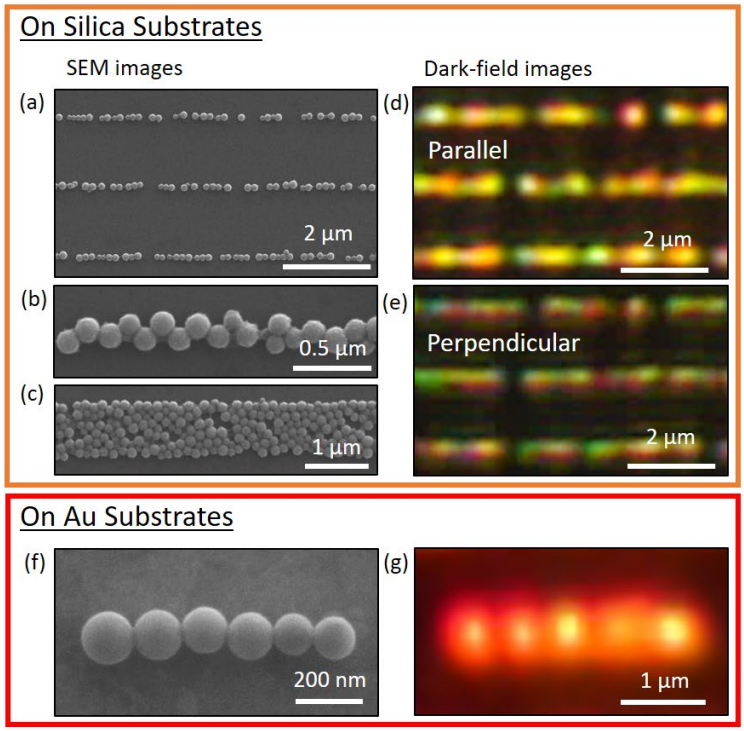

Figure 2. a-e) Si NP arrays on silica substrates. SEM images of a) linear arrays, b) a zigzag array and c) a 2D array. d, e) Dark-field scattering images of linear arrays of Si NPs on silica substrates in (a). The polarization direction is d) parallel and e) perpendicular to the array axis. f, g) Si NPs arrays on atomically-flat Au substrates. f) A SEM image of a linear array (hexamer). g) A dark-field scattering image of a linear array.

2.2. Light Scattering by Silicon Nanoparticle 1D Array

For linear arrays of Si NPs transferred onto a silica substrate, we conducted polarization-resolved scattering measurements by using the setup shown in **Figure 3**a.[47] A linear array of Si NPs is irradiated via a dark field condenser (N.A. = 0.8-0.95). Right before the condenser, a pinhole and a liner polarizer are inserted to define the direction and polarization direction of incident light with respect to the axis of a linear array.[47] The direction of incident light is perpendicular to the axis and the polarization direction is either parallel or perpendicular to

the axis as schematically shown in Figure 3b. Scattered light is collected by the bottom objective (100 ×, N.A. = 0.90).

Figure 3c-f shows the scattering spectra of a single Si NP and the linear arrays composed of different number of NPs. The scattering images and the SEM images are also shown in the figures. Corresponding calculated scattering spectra are shown in Figure 3g-j. For the simulations, fluctuation of Si NP diameters in an array seen in the SEM images is taken into account, although it does not significantly modify the scattering spectra as can be seen in the Supporting Information (Figure S2). The gaps between Si NPs are set to 2 nm because of the existence of native oxides on the surface. The irradiation and collection geometries mimic the experimental setup in Figure 3a, i.e., the incident angle is 75° and scattering light in the polar angle range of 0 to 64° is collected. The silica substrate is not considered for the simulation.

First, we look at the scattering spectra of a single Si NP (Figure 3c). ED and MD modes are clearly visible and the spectral shape agrees well with the simulations (Figure 3g). The intensity ratio of the ED and MD modes depends on the polarization of incident light. This appears as different scattering color as can be seen in the insets. The polarization dependence arises from different radiation patterns between ED and MD modes. [47]

Figure 3d-f shows scattering spectra of a dimer, a tetramer and a pentamer of Si NPs, respectively, and Figure 3h-j shows corresponding simulation spectra. The simulations reproduce the scattering spectra very well. Slight difference between experiments and simulations may arise from the existence of the substrate and imperfections in the structure of the arrays, e.g., slight deviation of a NP position from an array axis, which is not considered in the simulations. When the polarization direction is perpendicular to the array axis (blue curves), the spectral shape is only slightly modified by the formation of an array. Even in the pentamer, peaks similar to ED and MD modes of single Si NPs are recognized, although several new fine features appear. On the other hand, when the polarization direction is parallel

to the array axis, the spectral shape changes significantly and the scattering intensity largely increases. This is due to coupling of ED modes of NPs along the axis.

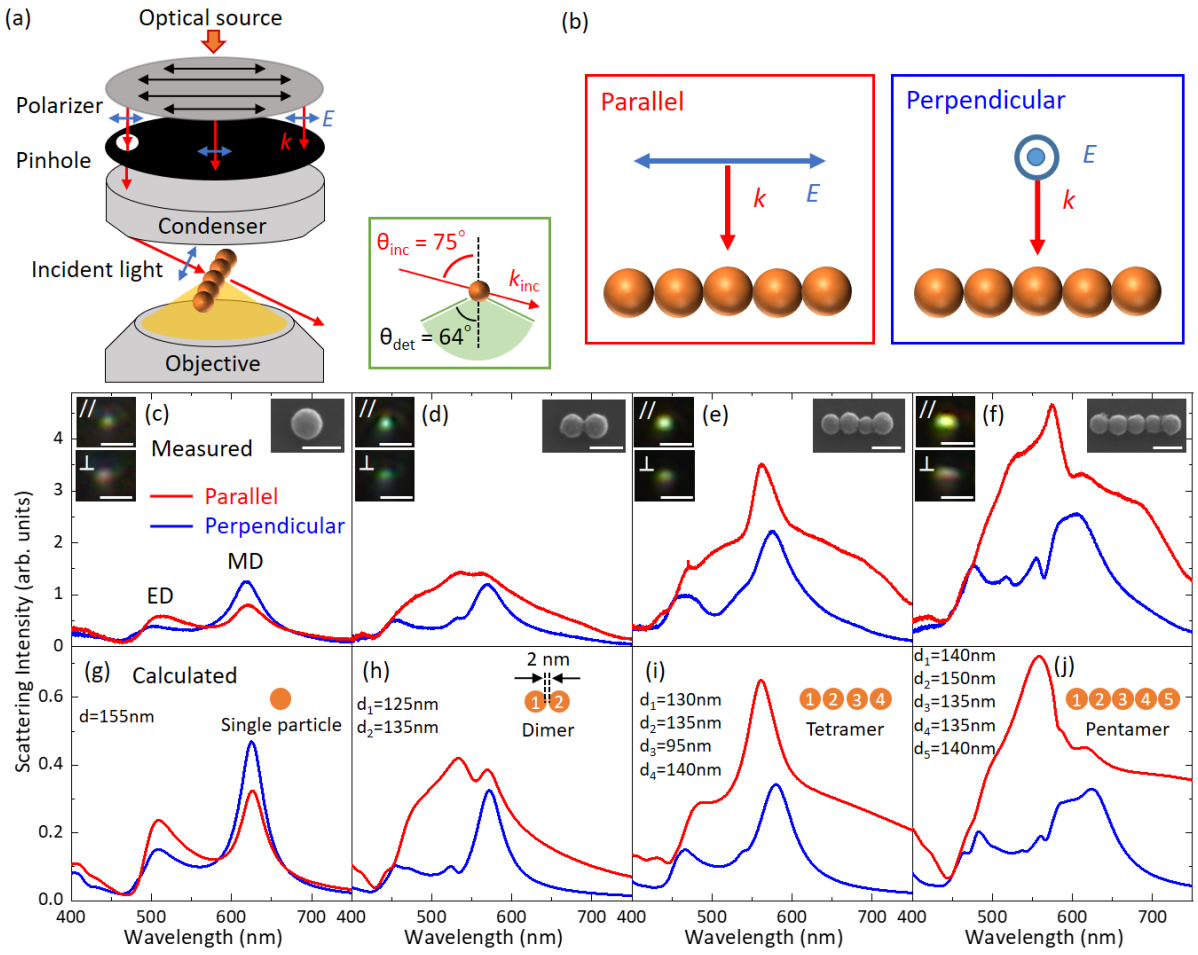

Figure 3. a) Schematic illustration of the scattering measurement setup. A Si NP array is irradiated via a polarizer, a pin hole and a dark-field condenser (N.A. = 0.8-0.95). The direction of incident light is perpendicular to the array axis. Blue arrows indicate the direction of electric field vectors. Scattered light is collected from the forward direction by an objective (NA: 0.9). The inset shows the incident and detection angles. b) Definition of parallel and perpendicular polarization directions. c-f) Measured scattering spectra for parallel and perpendicular polarizations; c) a monomer, d) a dimer, e) a tetramer and f) a pentamer of Si NPs. Insets show the scattering images for parallel (//) and perpendicular (⊥) polarizations and the SEM images. The scale bars are 1 μm for the scattering images and 200 nm for the

SEM images. g-j) Calculated scattering spectra corresponding to the experimental spectra in (c-f), respectively. Diameters of Si NPs estimated from the SEM images in (c-f) are used for the calculations and are shown in the figures. Gaps between Si NPs are set to 2 nm.

To unveil the mechanism of the spectral modification, we perform the multipole decomposition.[48] **Figure 4**a and b shows multipole contributions to the scattering spectra of a Si NP monomer (d = 135 nm) and the tetramer (Figure 3i), respectively, when the polarization direction is parallel to the array axis. The scattering spectrum of a Si NP monomer is dominated by ED and MD modes. The directions of the ED and MD moments and the electric field distribution at the peak wavelength of the ED mode (469 nm) are shown in Figure 4c. By the formation of a tetramer, the ED mode is strongly modified. It becomes very broad and the peak shifts to longer wavelength. Furthermore, the scattering intensity is strongly enhanced. Figure 4d shows the electric field distribution of the tetramer at the peak wavelength of the ED mode (559 nm). The electric field is localized at gaps between NPs and the peak intensity is more than 4 times larger than that of a Si NP monomer. This localization and enhancement of the ED mode is due to coupling of the ED moments of NPs oriented along the array axis.[15] It is noted that coupling of aligned ED moments occurs only when NPs are in very close proximity. In the Supporting Information (Figure S3), measured and simulated scattering spectra of Si NP dimers with different gap lengths are shown together with the electric field distributions. The scattering spectra and the field distributions are strongly modified from those of a Si NP monomer only when NPs are in contact. In Figure 4b, in contrast to the ED mode, the MD mode is not strongly affected by the formation of a tetramer. This is because the MD moments are aligned perpendicular to the axis.

Figure 4e and f shows the results of multipole decomposition of scattering spectra for a Si NP monomer and a tetramer, respectively, when the polarization direction is perpendicular to the array axis. Corresponding magnetic field distributions at the peaks of the MD modes are

shown in Figure 4g and h, respectively. In this case, the MD moments align along the array axis. However, in contrast to the ED mode under parallel polarization (Figure 4d), the magnetic field distribution of the MD mode is modified only slightly by the formation of the tetramer. Even though NPs are in very close proximity, the coupling is small and the field distribution is similar to that of individual NPs (Figure 4h). This is due to strong confinement of the magnetic field in a core of a sphere as can be seen in Figure 4g. Similar behavior is observed in Si NP linear arrays composed of different number of NPs (see Figure S4 in the Supporting Information).

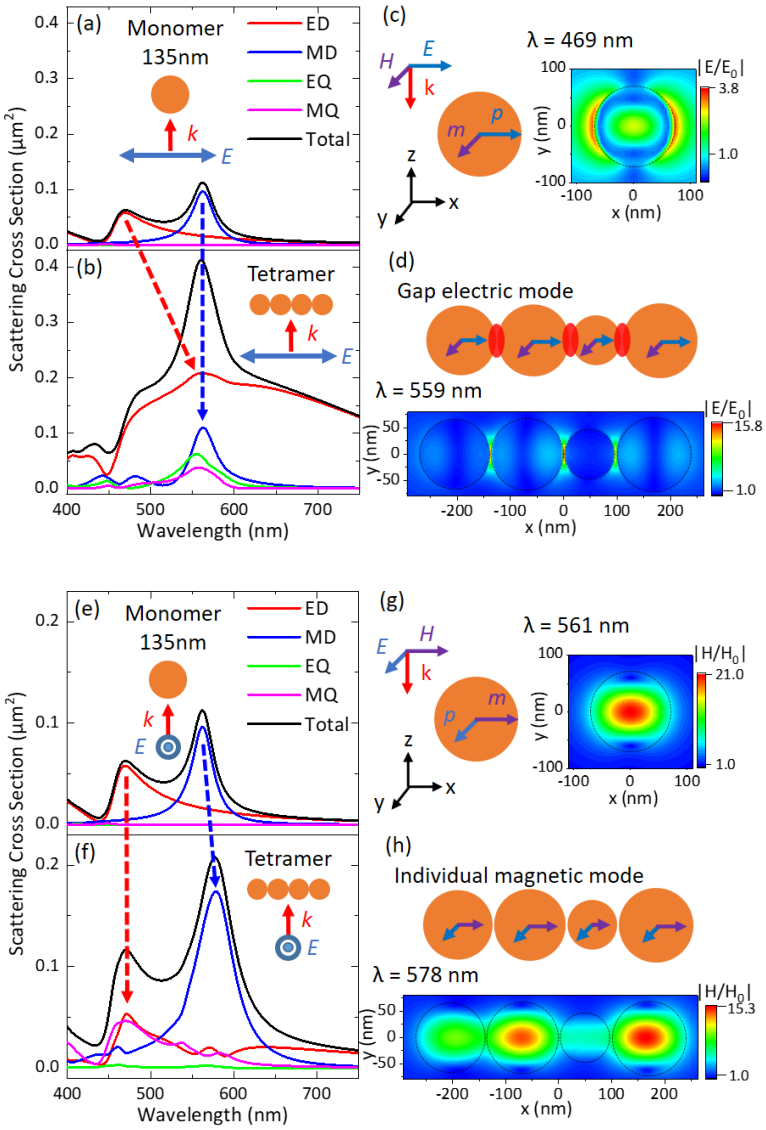

Figure 4. a, b) Multipole decomposition of the calculated scattering spectra into the contributions of ED, MD, EQ and MQ moments for a) a Si NP monomer (135 nm in diameter) and b) a tetramer for parallel polarization. The sizes of Si NPs in the tetramer are the same as those in Figure 3i. c, d) Electric field distributions of c) a Si NP monomer at 469 nm and d) a tetramer at 559 nm. These wavelengths correspond to the peak of the ED moment in (a) and (b). e, f) The same as (a, b) for perpendicular polarization. g, h) Magnetic field distributions of g) a Si NP monomer at 561 nm and h) a tetramer at 578 nm. These wavelengths correspond to the peak of the MD moments in (e) and (f).

2.3. Directional Scattering by Silicon Nanoparticles 1D Tetramer

It is well-known that, in a Si NP, the first Kerker condition, [49] i.e., the destructive interference of the radiation of the MD and ED modes to the backward (BW) direction and the constructive interference to the forward (FW) direction, is satisfied at a specific wavelength. **Figure 5**a shows calculated scattering spectra of a Si NP monomer to a FW hemisphere and to a BW hemisphere. A large FW to BW scattering contrast is achieved at the long wavelength tail of the MD mode. On the other hand, at the peak of the FW scattering (565 nm), the far field radiation pattern is almost isotropic (Figure 5b).

In linear arrays of Si NPs, the long wavelength shift of the ED mode improves the overlap with the MD modes, and thus strong directional (forward) scattering at the MD peak wavelength is expected. In Figure **5**c, calculated scattering spectra to FW and BW directions and the ratio (FW/BW) are shown for a Si NP tetramer (the same as that in Figure 3i). The polarization direction is parallel to the axis. The peak of the FW/BW ratio spectrum overlaps with that of the FW scattering spectrum, and thus high FW to BW scattering contrast (FW/BW: 9.0) is achieved at the peak of the FW scattering (561 nm) (Figure 5d).

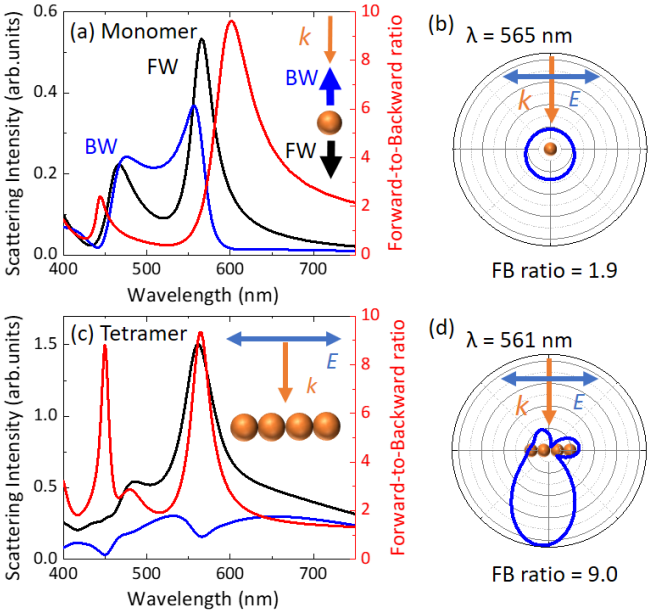

Figure 5. a) Calculated scattering spectra to FW and BW hemispheres for a Si NP monomer 135 nm in diameter. The right axis is the FW to BW scattering ratio spectrum. b) Far field radiation pattern at the peak of the FW scattering spectrum of a Si NP monomer (565 nm). (c) Calculated scattering spectra to FW and BW hemispheres for a Si NP tetramer. The diameter of NPs in the tetramer are the same as those in Figure 3i. The polarization direction is parallel to the tetramer axis. d) Far field radiation pattern at the peak of the FW scattering spectrum of the tetramer (561 nm).

In order to confirm the enhanced FW scattering in a Si NP tetramer, we measure the FW and BW scattering spectra by the setup shown in **Figure 6**a.[50] Figure 6b shows the FW and BW scattering spectra of the tetramer in Figure 3e. The FW scattering spectrum has a peak around 567 nm, and a relatively large FW/BW scattering ratio (3.8) is achieved at the peak wavelength, although the peaks of the forward scattering and the FW/BW ratio is slightly different. The observed FW/BW ratio is much larger than that of a Si NP monomer at the FW scattering peak measured by the same setup (1.1).

Figure 6c shows the scattering spectra calculated by mimicking the experimental irradiation and collection geometries in Figure 6a, i.e., the incident angle is 62.5° and scattering light in

the polar angle range of 0 to 53° is collected. A silica substrate is considered for the calculation. The spectral shape of the FW/BW ratio spectrum as well as the FW and BW scattering spectra is relatively well reproduced by the simulation. In the simulation, in contrast to that in Figure 5c, the peak of the FW/BW ratio spectrum does not perfectly agree with that of the FW scattering spectrum. This is due to the existence of silica substrate. In the Supporting Information, calculated scattering spectra with and without a silica substrate are compared (Figure S5), and the FW/BW ratio spectrum without the substrate is shown (Figure S6). Without the substrate, the FW/BW ratio peak agrees very well with the FW scattering one.

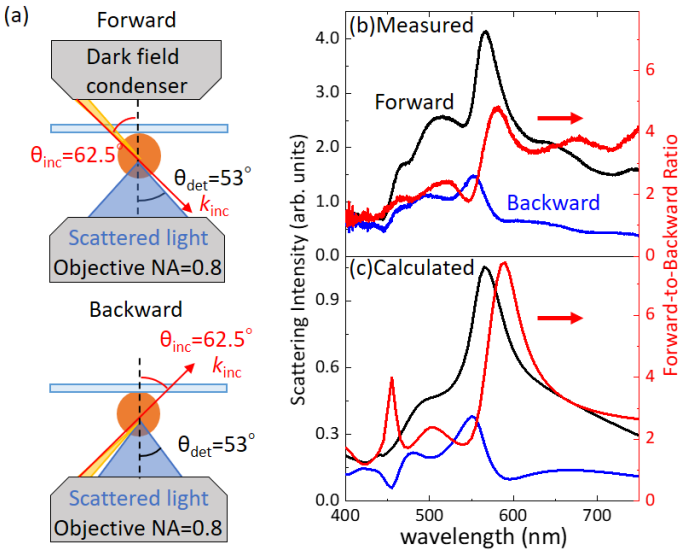

Figure 6. a) Schematic illustrations of the FW and BW scattering measurement setups. A Si NP array is illuminated via a pin hole and a dark-field condenser (N.A. = 0.8-0.95) for FW scattering measurements and via a pin hole and a dark-field objective (N.A. = 0.8) for BW scattering measurements. In both cases, the direction of incident light is perpendicular to an array axis and the polarization direction is parallel to the axis. b) Measured and c) calculated FW and BW scattering spectra and the ratio for a Si NP tetramer. The calculations mimic the experimental setups. A silica substrate is considered. The gaps between NPs and between a NP and a substrate are set to 2 nm.

3. Summary

We have developed a bottom-up process to produce arrays of crystalline Si NPs. We demonstrated the production of linear arrays, zig-zag arrays and 2D arrays of Si NPs from colloidal solution of Si NPs by a template-assisted self-assembly method, and their transfer to silica and Au substrates. We studied polarization-resolved scattering spectra of the linear arrays up to the pentamer and observed a systematic change of the scattering spectra with the length of the array due to the strong near-filed coupling of the ED modes. The arraying shifted the peak of the ED mode to longer wavelength and, in Si NP tetramer, it overlapped with the MD mode. This appeared as strong forward scattering around the MD peak wavelength due to the Kerker effect. In the template-assisted self-assembly process developed in this work, the gap between Si NPs can be reduced to nearly zero, which has significant advantages in some applications. For example, the propagation efficiency of a NP waveguide may be greatly improved. [51] Therefore, the structures produced by the present process provide new functionalities that are hard to be realized by conventional micro-fabrication technology.

4. Experimental Section

Preparation of a water solution of colloidal silicon nanoparticles: Si NPs were synthesized by thermal disproportionation of SiO and subsequent etching by a HF solution.[39,40] SiO lumps (Kojundo Chemical Lab, 99.99 %) were crushed to powder and annealed at 1475 °C in a N_2 gas atmosphere for 30 min to grow crystalline Si NPs in SiO_2 matrices. Si NPs were extracted from a matrix by etching in a HF solution (46 wt %) for 1 h, transferred to methanol and subjected to sonication with an ultrasonic homogenizer (Violamo SONICSTAR 85) for a minute. For size separation of Si NPs, sucrose density gradient centrifugation process was employed.[39] First, sucrose solutions with three different concentrations (45, 42.5, and 40 wt %) were added to a centrifugal tube in order. Then, water solution of Si NPs was carefully

dropped on the sucrose solution and centrifuged at 4000 rpm for 40 min. By extracting a desired region of the solution in the tube, size-separated Si NPs were obtained. Finally, Si NPs were washed with water several times to remove sucrose.

Preparation of templates for template-assisted self-assembly: Polydimethylsiloxane (PDMS) mold was fabricated as a replica of a master mold (a quartz nanoimprint mold, NTT Advanced Technology Corp NIMPHL80 18-0131)) by a pressure-assisted molding process.[52] The mold pattern is transcribed to photopolymer (Toyogosei PAK-01) spin-coated on a polymethyl methacrylate (PMMA)-coated Si wafer by UV nanoimprint.

Template-assisted self-assembly of Si NPs: A home-made system composed of a motorized linear stage for pulling a template, a z-axis stage to control a template-cover glass distance, a thermoelectric cooler, and a humidistat bath is used. The volume and density of Si NP solution, the velocity of a template, the template-cover glass distance, the solution temperature and the relative humidity were 20 µl, ~0.1 mg mL^{-1}, 4.0 µm s^{-1}, 1 mm, 15 °C and 43 %, respectively.

Transfer of Si NPs arrays to a substrate: Cellulose acetate butyrate (Sigma-Aldrich average MW = 70,000) was dissolved in ethyl acetate (30 mg mL^{-1}) [53] and the solution was dropped on a template and dried in air for 10 min to form a CAB film. The film was detached from the template in water and placed on a substrate treated by a UV ozone cleaner (SAMCO UV-1) to hydrophilize the surface. Finally, a CAB film was dissolved by ethyl acetate.

Preparation of ultraflat Au film: An ultraflat Au film was prepared on a silica substrate by the template-stripping method by using a Si wafer as a template.[46][54]

Scattering measurement of single Si NPs arrays: A custom-built inverted optical microscope connected to an imaging spectrometer (Kymera 328i Oxford Instruments) and a charge coupled device was used for dark-field scattering measurements of single Si NPs arrays. For BW scattering measurements, spectral response of the system was corrected by the scattering

spectrum of a diffuse reflectance standard (Spectralon PP-100-SL), while for FW scattering measurements, it was corrected by the spectrum of a transmitted light from a halogen lamp.

Forward and backward scattering measurements: FW and BW scattering spectra were obtained by the setup shown in Figure 6a. We obtained the correction factor for FW and BW scattering intensities in the experimental setup by comparing the experimental and calculated spectra of a single Si NP (Figure S7 in the Supporting Information).

Numerical Simulation: Calculation of scattering spectra and electric and magnetic field distributions was performed by using a finite-difference time-domain method (Lumerical, Ansys). The complex dielectric permittivity of Si was taken from Palik.[55] The simulated box consisted of perfectly matched layer (PML) boundaries and a total-field scattering-field (TFSF) source was employed to calculate scattering spectra.

Supporting Information

Supporting Information is available from the Wiley Online Library or from the author.

Acknowledgements

H S acknowledge the supported by JST, PRESTO Grant Number JPMJPR19T4, Japan. This work is partly supported also by JSPS KAKENHI Grant Numbers 18KK0141, 21H01748, 21H01782 and 21K14496.

Received: ((will be filled in by the editorial staff))
Revised: ((will be filled in by the editorial staff))
Published online: ((will be filled in by the editorial staff))

References

[1] Z.-J. Yang, R. Jiang, X. Zhuo, Y.-M. Xie, J. Wang, H.-Q. Lin, *Phys. Rep.* **2017**, *701*, 1.

[2] G. Yang, Y. Niu, H. Wei, B. Bai, H.-B. Sun, *Nanophotonics* **2019**, *8*, 2313.

[3] R. Regmi, J. Berthelot, P. M. Winkler, M. Mivelle, J. Proust, F. Bedu, I. Ozerov, T. Begou, J. Lumeau, H. Rigneault, M. F. García-Parajó, S. Bidault, J. Wenger, N. Bonod, *Nano Lett.* **2016**, *16*, 5143.

[4] H. Sugimoto, M. Fujii, *ACS Photonics* **2021**, acsphotonics.1c00375.

[5] A. Krasnok, S. Glybovski, M. Petrov, S. Makarov, R. Savelev, P. Belov, C. Simovski, Y. Kivshar, *Appl. Phys. Lett.* **2016**, *108*, 1.

[6] M. Decker, I. Staude, M. Falkner, J. Dominguez, D. N. Neshev, I. Brener, T. Pertsch, Y. S. Kivshar, *Adv. Opt. Mater.* **2015**, *3*, 813.

[7] G. Lee, J. Sung, B. Lee, *MRS Bull.* **2020**, 202.

[8] A. E. Krasnok, A. E. Miroshnichenko, P. A. Belov, Y. S. Kivshar, *Opt. Express* **2012**, *20*, 837.

[9] R. M. Bakker, Y. F. Yu, R. Paniagua-Domínguez, B. Luk'yanchuk, A. I. Kuznetsov, *Nano Lett.* **2017**, *17*, 3458.

[10] T. Hinamoto, M. Fujii, T. Sannomiya, *Opt. Express* **2021**, *29*, 34951.

[11] R. Paniagua-Domínguez, Y. F. Yu, E. Khaidarov, S. Choi, V. Leong, R. M. Bakker, X. Liang, Y. H. Fu, V. Valuckas, L. A. Krivitsky, A. I. Kuznetsov, *Nano Lett.* **2018**, *18*, 2124.

[12] E. Panagiotidis, E. Almpanis, N. Stefanou, N. Papanikolaou, *J. Appl. Phys.* **2020**, *128*, 093103.

[13] E. Khaidarov, H. Hao, R. Paniagua-Domínguez, Y. F. Yu, Y. H. Fu, V. Valuckas, S. L. K. Yap, Y. T. Toh, J. S. K. Ng, A. I. Kuznetsov, *Nano Lett.* **2017**, *17*, 6267.

[14] G.-Y. Lee, J. Hong, S. Hwang, S. Moon, H. Kang, S. Jeon, H. Kim, J. Jeong, B. Lee, *Nat. Commun.* **2018**, *9*, 4562.

[15] J. H. Yan, P. Liu, Z. Y. Lin, H. Wang, H. J. Chen, C. X. Wang, G. W. Yang, *Nat. Commun.* **2015**, *6*, 7042.

[16] P. Albella, M. A. Poyli, M. K. Schmidt, S. A. Maier, F. Moreno, J. J. Sáenz, J. Aizpurua, *J. Phys. Chem. C* **2013**, *117*, 13573.

[17] U. Zywietz, M. K. Schmidt, A. B. Evlyukhin, C. Reinhardt, J. Aizpurua, B. N. Chichkov, *ACS Photonics* **2015**, *2*, 913.

[18] M. Naffouti, T. David, A. Benkouider, L. Favre, M. Cabie, A. Ronda, I. Berbezier, M. Abbarchi, *Nanotechnology* **2016**, *27*, DOI: 10.1088/0957-4484/27/30/305602.

[19] J. Ye, D. Zuev, S. Makarov, *Int. Mater. Rev.* **2019**, *64*, 439.

[20] M. Abbarchi, M. Naffouti, B. Vial, A. Benkouider, L. Lermusiaux, L. Favre, A. Ronda, S. Bidault, I. Berbezier, N. Bonod, *ACS Nano* **2014**, *8*, 11181.

[21] M. Naffouti, T. David, A. Benkouider, L. Favre, A. Delobbe, A. Ronda, I. Berbezier, M. Abbarchi, *Small* **2016**, *12*, 6115.

[22] P. A. Dmitriev, S. V. Makarov, V. A. Milichko, I. S. Mukhin, A. S. Gudovskikh, A. A. Sitnikova, A. K. Samusev, A. E. Krasnok, P. A. Belov, *Nanoscale* **2016**, *8*, 5043.

[23] U. Zywietz, A. B. Evlyukhin, C. Reinhardt, B. N. Chichkov, *Nat. Commun.* **2014**, *5*, 3402.

[24] L. Shi, J. T. Harris, R. Fenollosa, I. Rodriguez, X. Lu, B. A. Korgel, F. Meseguer, *Nat. Commun.* **2013**, *4*, 1904.

[25] N. Vogel, M. Retsch, C.-A. Fustin, A. del Campo, U. Jonas, *Chem. Rev.* **2015**, *115*, 6265.

[26] Y. Yin, Y. Lu, B. Gates, Y. Xia, *J. Am. Chem. Soc.* **2001**, *123*, 8718.

[27] Takashi Ozaki, Koji Sugano, Toshiyuki Tsuchiya, Osamu Tabata, in *2007 IEEE 20th Int. Conf. Micro Electro Mech. Syst.*, IEEE, **2007**, pp. 353–356.

[28] M. Mayer, P. L. Potapov, D. Pohl, A. M. Steiner, J. Schultz, B. Rellinghaus, A. Lubk, T. A. F. König, A. Fery, *Nano Lett.* **2019**, *19*, 3854.

[29] P. T. Probst, M. Mayer, V. Gupta, A. M. Steiner, Z. Zhou, G. K. Auernhammer, T. A. F. König, A. Fery, *Nat. Mater.* **2021**, *20*, 1024.

[30] J. B. Lee, H. Walker, Y. Li, T. W. Nam, A. Rakovich, R. Sapienza, Y. S. Jung, Y. S. Nam, S. A. Maier, E. Cortés, *ACS Nano* **2020**, *14*, 17693.

[31] S. Ni, J. Leemann, I. Buttinoni, L. Isa, H. Wolf, *Sci. Adv.* **2016**, *2*, e1501779.

[32] H. Sugimoto, M. Fujii, *Adv. Photonics Res.* **2021**, *2000111*, 2000111.

[33] L. Shi, T. U. Tuzer, R. Fenollosa, F. Meseguer, *Adv. Mater.* **2012**, *24*, 5934.

[34] A. B. Evlyukhin, S. M. Novikov, U. Zywietz, R. L. Eriksen, C. Reinhardt, S. I. Bozhevolnyi, B. N. Chichkov, *Nano Lett.* **2012**, *12*, 3749.

[35] W. Chaâbani, J. Proust, A. Movsesyan, J. Béal, A.-L. Baudrion, P.-M. Adam, A. Chehaidar, J. Plain, *ACS Nano* **2019**, *13*, 4199.

[36] R. M. Bakker, D. Permyakov, Y. F. Yu, D. Markovich, R. Paniagua-Domínguez, L. Gonzaga, A. Samusev, Y. Kivshar, B. Luk'yanchuk, A. I. Kuznetsov, *Nano Lett.* **2015**, *15*, 2137.

[37] J. Cambiasso, G. Grinblat, Y. Li, A. Rakovich, E. Cortés, S. A. Maier, *Nano Lett.* **2017**, *17*, 1219.

[38] T. Shibanuma, T. Matsui, T. Roschuk, J. Wojcik, P. Mascher, P. Albella, S. A. Maier, *ACS Photonics* **2017**, *4*, 489.

[39] H. Sugimoto, T. Okazaki, M. Fujii, *Adv. Opt. Mater.* **2020**, *8*, 2000033.

[40] T. Okazaki, H. Sugimoto, T. Hinamoto, M. Fujii, *ACS Appl. Mater. Interfaces* **2021**, *13*, 13613.

[41] L. Malaquin, T. Kraus, H. Schmid, E. Delamarche, H. Wolf, *Langmuir* **2007**, *23*, 11513.

[42] J. J. Mock, R. T. Hill, A. Degiron, S. Zauscher, A. Chilkoti, D. R. Smith, *Nano Lett.* **2008**, *8*, 2245.

[43] A. Rose, T. B. Hoang, F. McGuire, J. J. Mock, C. Ciracì, D. R. Smith, M. H. Mikkelsen, *Nano Lett.* **2014**, *14*, 4797.

[44] I. Sinev, I. Iorsh, A. Bogdanov, D. Permyakov, F. Komissarenko, I. Mukhin, A. Samusev, V. Valuckas, A. I. Kuznetsov, B. S. Luk'yanchuk, A. E. Miroshnichenko, Y. S. Kivshar, *Laser Photonics Rev.* **2016**, *10*, 799.

[45] H. Sugimoto, M. Fujii, *ACS Photonics* **2018**, *5*, 1986.

[46] H. Sugimoto, R. Imaizumi, T. Hinamoto, T. Kawashima, M. Fujii, *ACS Appl. Nano Mater.* **2020**, *3*, 7223.

[47] T. Hinamoto, M. Hamada, H. Sugimoto, M. Fujii, *Adv. Opt. Mater.* **2021**, *9*, 2002192.

[48] T. Hinamoto, M. Fujii, *OSA Contin.* **2021**, *4*, 1640.

[49] M. Kerker, D.-S. Wang, C. L. Giles, *J. Opt. Soc. Am.* **1983**, *73*, 765.

[50] H. Sugimoto, T. Hinamoto, M. Fujii, *Adv. Opt. Mater.* **2019**, *7*, 1.

[51] R. S. Savelev, A. P. Slobozhanyuk, A. E. Miroshnichenko, Y. S. Kivshar, P. A. Belov, *Phys. Rev. B* **2014**, *89*, 035435.

[52] N. Koo, U. Plachetka, M. Otto, J. Bolten, J. Jeong, E. Lee, H. Kurz, *Nanotechnology* **2008**, *19*, 225304.

[53] N. S. King, M. W. Knight, N. Large, A. M. Goodman, P. Nordlander, N. J. Halas, *Nano Lett.* **2013**, *13*, 5997.

[54] P. Nagpal, N. C. Lindquist, S.-H. Oh, D. J. Norris, *Science (80-.).* **2009**, *325*, 594.

[55] E. D. Palik, *Handbook of Optical Constants of Solids*, Academic Press, Boston, **1998**.

A bottom-up process to produce linear, zig-zag and two-dimensional arrays of densely-packed spherical nanoparticles of crystalline silicon from the solution are developed, and the polarization-resolved scattering properties of the linear arrays are studied systematically from the dimer to the pentamer. Enhanced forward scattering in an array due to better overlap of the electric dipole and magnetic dipole modes is also discussed.

Hidemasa Negoro, [†] Hiroshi Sugimoto, [†,‡] Tatsuki Hinamoto, [†]and Minoru Fujii*[,†]

Template-Assisted Self-Assembly of Colloidal Silicon Nanoparticles for All-Dielectric Nanoantenna